Nussbaum *et al. Veterinary Oncology* (2025) 2:25
https://doi.org/10.1186/s44356-025-00037-0

Veterinary Oncology

RESEARCH Open Access

Comparative multi-omics evaluation of the tumor microenvironment in dog and human hepatocellular carcinoma

Yulia I. Nussbaum[1], Jeffrey N. Bryan[2], Guangfu Li[11], Alana Rodney[3], William T. N. Culp[4], Peter J. Dickinson[4], Anna Koutoulas[5], Kate Megquier[5], Hong An[6], Skyler T. Kramer[1,6], Edward S. Ricemeyer[7,8], Jonathan B. Mitchem[9] and Wesley C. Warren[1,7,10*]

Abstract

Background Dog hepatocellular carcinoma (HCC) is the most common primary liver tumor in dogs, though it remains relatively rare overall. In humans HCC is frequently resistant to chemotherapy and radiation and often shows insufficient response to immunotherapy. Its occurrence in dogs, unlike humans, is not typically associated with viral infections, cirrhosis, or alcohol consumption. These distinctions offer a unique comparative perspective on the intrinsic genetic drivers of the disease.

Methods Using whole exome sequencing (WES) and single nucleus RNA sequencing (snRNA-seq) in tandem, we perform a multi-omic analysis of the dog HCC tumor.

Results Mutational analysis of impactful polymorphisms revealed a conserved cross-species landscape with genes such as *CTNNB1*, known for highly recurrent mutations in human HCC, showing similar alterations in dogs. In dog HCC tumors, we identified the major cell types commonly observed in human HCC, including T cells, endothelial, macrophage, fibroblast, hepatocyte, and malignant characterizations. The inferred cellular communication observed across human and dog HCC cell types revealed parallels, particularly in macrophage functionality.

Conclusions These findings underscore the need for expanded genetic studies of dog HCC to further elucidate cross-species commonalities, offering deeper insights into key aspects of HCC biology and identifying novel therapeutic targets.

Keywords Hepatocellular carcinoma, Canine cancer, Comparative oncology, scRNA-seq data, Tumor microenvironment

*Correspondence:
Wesley C. Warren
warrenwc@missouri.edu

Full list of author information is available at the end of the article

Introduction

Human HCC is the most common primary liver cancer and remains a major global health challenge, accounting for approximately 90% of liver cancer cases. Its incidence is projected to surpass 1 million cases annually by 2025 [1, 2]. Despite advances in systemic therapies, the overall prognosis for HCC remains poor largely due to its late presentation, complex tumor microenvironment (TME), and a high degree of treatment resistance [3]. However, significant advances in the use of immune checkpoint inhibitors are transforming treatment paradigms. Notably, the combination of atezolizumab and bevacizumab has shown improved overall survival compared to sorafenib, while other combinations like durvalumab and tremelimumab and atezolizumab plus cabozantinib have also demonstrated efficacy [4, 5]. But patients still fail to respond to these therapies, and the molecular mechanisms governing immune resistance and evasion remain incompletely understood [6, 7]. Further research is needed to deepen our understanding of HCC biology and guide the development of effective immunotherapies.

One promising avenue to break this treatment impasse is through the study of the only spontaneous animal that gets HCC, dogs [8, 9]. Unlike murine models, which are induced and often fail to replicate the complexity of human disease, dog cancers arise spontaneously, maintaining intact immune systems and recapitulating tumor-immune interactions within a naturally evolving TME [10, 11]. Over the past decade, significant advances in cancer research have shown that dog cancers closely resemble human cancers in prevalence, tumor growth patterns, morphology, and genetic foundations [12–17]. This parallel has renewed interest in applying best-practice human therapeutics to dog patients, particularly in the realm of immunotherapy. Precision oncology initiatives underscore the importance of tailoring treatment strategies to an individual's complex molecular and immune TME to achieve lasting tumor suppression [18]. Across nearly all cancer types, large-scale analyses of somatic mutations and cell-type composition within the TME have deepened our understanding of their cooperative roles in tumor progression [19, 20].

HCC is the most common primary liver tumor in dogs, similar to humans. Although massive HCC in dogs tends to be slow-growing and less metastatic, it shares key histological and molecular features with human HCC, including frequent mutations in TP53, CTNNB1, and ARID1A, and altered Wnt/β-catenin and DNA repair pathways [2, 21, 22]. While surgical resection is the primary treatment for dog HCC, there is a need to improve systemic options such as chemotherapy and explore immunotherapy, which is currently limited. Better understanding the molecular similarities between dog and human HCC could accelerate the development of novel treatments for both species.

Single-cell RNA sequencing (scRNA-seq) has emerged as a powerful tool to dissect cellular composition of tumors and, importantly, to identify which cell types represent high-value therapeutic targets [23, 24]. Its repeated use has provided insights into cellular subtypes, immune evasion mechanisms, and potential biomarkers predictive of prognosis or treatment response. Recent studies underscore the ability to stratify therapies for various cancer types. For example, scRNA-seq data analysis has uncovered distinct populations of neutrophils that present novel opportunities for HCC immunotherapy [25]. Thus far, the observed cellular landscape of human HCC emphasizes the importance of malignant cells in shaping the TME and identifying non-malignant cellular subtypes that can predict HCC prognosis [26]. Distinct functional compositions and varying molecular signatures have been identified across T cell subtypes [27], revealing a unique immune ecosystem in early-relapse HCC, characterized by decreased regulatory T cells, and increased dendritic and CD8 + T cells [28]. Furthermore, several studies have identified prognostic cell type compositional shifts in HCC tumors including a tumor-associated proliferative cell type enriched in expression of cell cycle and mitosis genes, subsets of cancer-associated fibroblasts (CAFs), and M2-like tumor-associated macrophages (TAMs) [29–31].

These collective findings of the TME have also added new testable hypotheses regarding the mechanisms of immunotherapy resistance in HCC. Inhibition of apolipoprotein C1, which is overexpressed in TAMs, promoted transformation of M2 macrophages to M1 type, thereby improving anti-PD1 therapy [32]. Similarly, the targeting of PPAR-gamma has been shown to counteract tumor adaptation to immune-checkpoint blockade [33]. One study identified new subtypes of HCC tumor cells and neutrophils with potential implications for immunotherapy research while also inferring a complex intercellular communication was at work in the tumor [25].

To our knowledge, no studies to date have used dog HCC-specific multi-omic datasets, such as somatic mutation profiles and single-cell or single-nucleus transcriptomes of the TME. Such efforts could facilitate the repurposing of human treatment strategies for canine patients and advance the study of spontaneous dog cancers with variable outcomes. This includes enabling clinical trials of immunotherapies and identifying novel biomarkers predictive of treatment response [16, 17, 34]. To begin addressing this gap, we collected and analyzed two data types, WES and snRNA-seq, from a small cohort of dog HCC cases and compared findings with analogous human HCC data. Our analysis reveals shared driver mutations and TME features between species,

providing foundational insights and establishing a framework for future cross-species studies. Although preliminary, these findings lay important groundwork for advancing comparative oncology and guiding therapeutic development in both human and veterinary medicine.

Methods

Study animals

All dog tumor samples were classified as HCC based on previously accepted histopathological diagnosis criteria [35]. All tumor and normal blood samples were obtained under studies approved by the University of California, Davis or University of Missouri Institutional Animal Care and Use Committees. We complied with all relevant ethical regulations for animal use and all dog owners provided informed consent prior to sample collection. WES was performed on HCC tumors and matched blood from ten dogs (Suppl. Table 1) from which two were chosen for snRNA-seq data generation based on the availability of flash frozen HCC biopsies (Suppl. Table 1).

WES library construction

For all tumor samples we isolated total DNA using the DNA easy kit (Qiagen) from the liver tumor tissue and the matching blood samples. A total of 2ug DNA served as the input for acoustic DNA fragmentation using a Covaris focused-ultrasonicator, targeting 150 bp fragments. Library preparation was performed using a commercially available kit provided by KAPA Biosystems (KAPA HyperPrep Kit with Library Amplification product KK8504) and IDT's duplex UMI adapters. Unique 8-base dual index sequences embedded within the p5 and p7 primers (IDT) were added during PCR. Enzymatic clean-ups were performed using Beckman Coultier AMPure XP beads with elution volumes reduced to 30μL to maximize library concentration. Final library quantification was performed using the Invitrogen Quant-It broad range dsDNA quantification assay kit (Thermo Scientific Catalog: Q33130) with a 1:200 PicoGreen dilution. Following quantification, each library was normalized to a concentration of 35 ng/μL, using Tris-HCl, 10mM, pH 8.0.

In-solution hybrid selection for exome or custom panels

After library construction, hybridization and capture were performed using IDT's XGen hybridization and wash kit and following the manufacturer's suggested protocol, with minor exceptions. Briefly, a set of 12-plex pre-hybridization pools was created by equal volume pooling of the normalized libraries, human Cot-1, and IDT XGen blocking oligos. The pre-hybridization pools underwent lyophilization using the Biotage SPE-DRY. Post lyophilization, Twist Alliance Canine Exome baits (Twist Biosciences, San Francisco, CA) along with hybridization master mix were added to the lyophilized pool prior to resuspension and samples were incubated overnight. Library normalization and hybridization setup were performed on a Hamilton Starlet liquid handling platform, while target capture was performed on the Agilent Bravo automated platform. Post capture, PCR was performed to amplify the captured material. After post-capture enrichment, library pools were quantified using qPCR (automated assay on the Agilent Bravo), using a kit purchased from KAPA Biosystems with probes specific to the ends of the adapters. Based on qPCR quantification, pools were normalized to 2nM prior to sequencing using a Hamilton Starlet.

Cluster amplification and sequencing

Cluster amplification of library pools was performed according to the manufacturer's protocol (Illumina) using Exclusion Amplification cluster chemistry and HiSeq X flowcells. Flowcells were sequenced using v2 Sequencing-by-Synthesis chemistry for HiSeq X flowcells. The flowcells were then analyzed using RTA v.2.7.3 or later. Each pool of libraries had paired 151 bp runs and was sequenced across the number of lanes needed to meet coverage for all libraries in the pool.

WES and variant analysis

Exome sequences from each tumor and matched normal samples were aligned to the UU_Cfam_GSD_1.0 dog genome [36]. Our variant data analysis pipeline used hisat2 (version 2.2.1) for initial alignment, and then GATK MarkDuplicates was applied to flag the reads that came from PCR duplication [37, 38]. All the normal samples were run with Mutect2 in tumor-only mode and used to construct the somatic panel of normals with the GATK CreateSomaticPanelOfNormals function. Single nucleotide variants (SNVs) and insertions/deletions (indels) calling was performed using GATK Mutect2 best practices (version 4.3.0.0) [38]. The tumor samples were run with their matched normal samples while using the panel of normals to aid in variant filtration. Variants were filtered with GATK FilterMutectCalls using default parameters and further filtered to retain calls with genotype missing rates < 0.01 and minor allele frequency (MAF) > 0.01. Finally, the functional effects of SNVs and INDELs were annotated using the Variant Effect Predictor (VEP) v109 based on the UU_Cfam_GSD_1.0_ROSY genome and its corresponding genome annotation file [39].

The tumor mutation burden (TMB)

The TMB per each sample was estimated as the ratio of nonsynonymous mutations to the total size of the sequenced exome (45 Mb in this study), as described previously [40].

Human WES and TMB data

Human HCC mutation data were retrieved from the COSMIC database (v97, https://cancer.sanger.ac.uk/cosmic) [41]. We filtered the data to include only coding mutations from confirmed HCC samples (tissue type: liver, histology: hepatocellular carcinoma). Only mutations labeled as somatic and validated by whole-exome or genome sequencing were retained. TMB values used for comparative analysis were obtained from previously published studies [42–45].

snRNA-seq sample processing and nuclei extraction

Snap-frozen tumor tissues were minced on ice and homogenized using a dounce homogenizer in cold Nuclei PURE Lysis Buffer (Millipore-Sigma) containing 0.1% Triton X-100 and 0.2 U/μL RNase inhibitor (Promega). Homogenate was transferred through 70 μm cell strainer and homogenized again a few strokes and passed through a 40 μm cell strainer. Filtrate was centrifuged at 500 g for 5 min at 40 C and the pellet was re-suspended in PBS with 0.4% UltraPure BSA (ThermoFisher Scientific) and 0.2 U/μL Protector RNase inhibitor (MilliporeSigma). This step was repeated, and the final resuspended nuclei were counted after staining with Propidium iodide using a Countess II instrument (ThermoFisher Scientific).

Library preparation and sequencing

Single-nuclei 3' RNA-seq library preparation and sequencing were conducted at the University of Missouri DNA Core Facility. Nuclei were counted and loaded onto the 10x Genomics Chromium System, targeting 5,000 nuclei per sample. After lipid droplet encapsulation, cDNA synthesis, and library preparation were performed following the manufacturer's protocol using the Chromium Next GEM Single Cell 3' v3.1 Kit. Sequencing was carried out on an Illumina NovaSeq 6000 instrument (University of Missouri Genomics Technology Core), with a target depth of 40,000 reads per nucleus.

snRNAseq data processing

Cellranger mkfastq was used for demultiplexing of raw sequencing files. Each sample was separately aligned to the CanFam3.1 reference genome using cellranger count, and all further analyses were performed using the Seurat V4.2.0 package [46, 47]. Quality control included filtering out dead or poor-quality nuclei according to the percentage of mitochondrial genes. The percentage of reads mapped to mitochondrial chromosomes per cell ("percent.MT") was calculated using PercentageFeatureSet() to count all reads mapped to features with the prefix "MT-". Each object was filtered to only retain nuclei which met the following criteria: >12,000 unique molecular identifier (UMI) counts; a range of 500 to 5,000 detected genes; < 1% of mitochondrial or ribosomal gene expression in UMI counts. From the filtered nuclei, the gene expression matrices were normalized using SCTransform (Pearson residuals of regularized negative binomial regression) and integrated into one object using Seurat's alignment workflow [48, 49]. The integrated object was then clustered using an optimal resolution parameter of 0.3 that was selected via clustree R package [50]. Next, using non-linear dimensionality reduction function RunUMAP we visualized the nuclei in two-dimensional UMAP plots.

Cell type identification

To identify the differentially expressed genes (DEGs) that uniquely characterize each cluster, we used the FindAllMarkers function of the Seurat package with the Wilcoxon Rank Sum test. Based on the individual cluster DEGs, cell type annotation was performed by manual curation with the use of lineage-specific canonical markers of known cell types in the human liver and dog leukocytes (Suppl. Table 2) [14, 51, 52].

Comparison of human and dog snRNA-seq data sets

Two treatment-naive human HCC samples were obtained from the NCBI GEO database accession number GSE189175 [29]. To integrate the human and dog snRNA-seq data, we utilized the scVI Python package [53]. The latent embeddings output by scVI were then used for graph-based clustering and dimensionality reduction using UMAP in Seurat V4.

Cancer stemness gene set

Cancer stemness of each nuclei cluster was scored per nuclei by gene set variation analysis (GSVA) based on the cancer stemness signature from Miranda et al. [54].

Cell-to-cell interaction inference analysis

To analyze ligand-receptor interactions in dog samples we used CellPhoneDB with a 'statistical_analysis' parameterization [55]. Using a curated list of known human receptor-ligand pairs from CellPhoneDB, we calculated interaction scores—representing the strength and probability of interactions between cell pairs. This method identifies interactions where the mean expression of the interacting proteins is significantly specific to cell states, employing a random shuffling approach for statistical inference. The analysis was performed across all seven identified cell types in dog HCC. Interactions were ranked based on average expression values, and the top interactions were visualized using the ComplexHeatmap R package (version 2.20.0).

Results

Sample biobanking and processing

An overview of the experimental design is displayed in Fig. 1A. All resected liver tumors analyzed by a

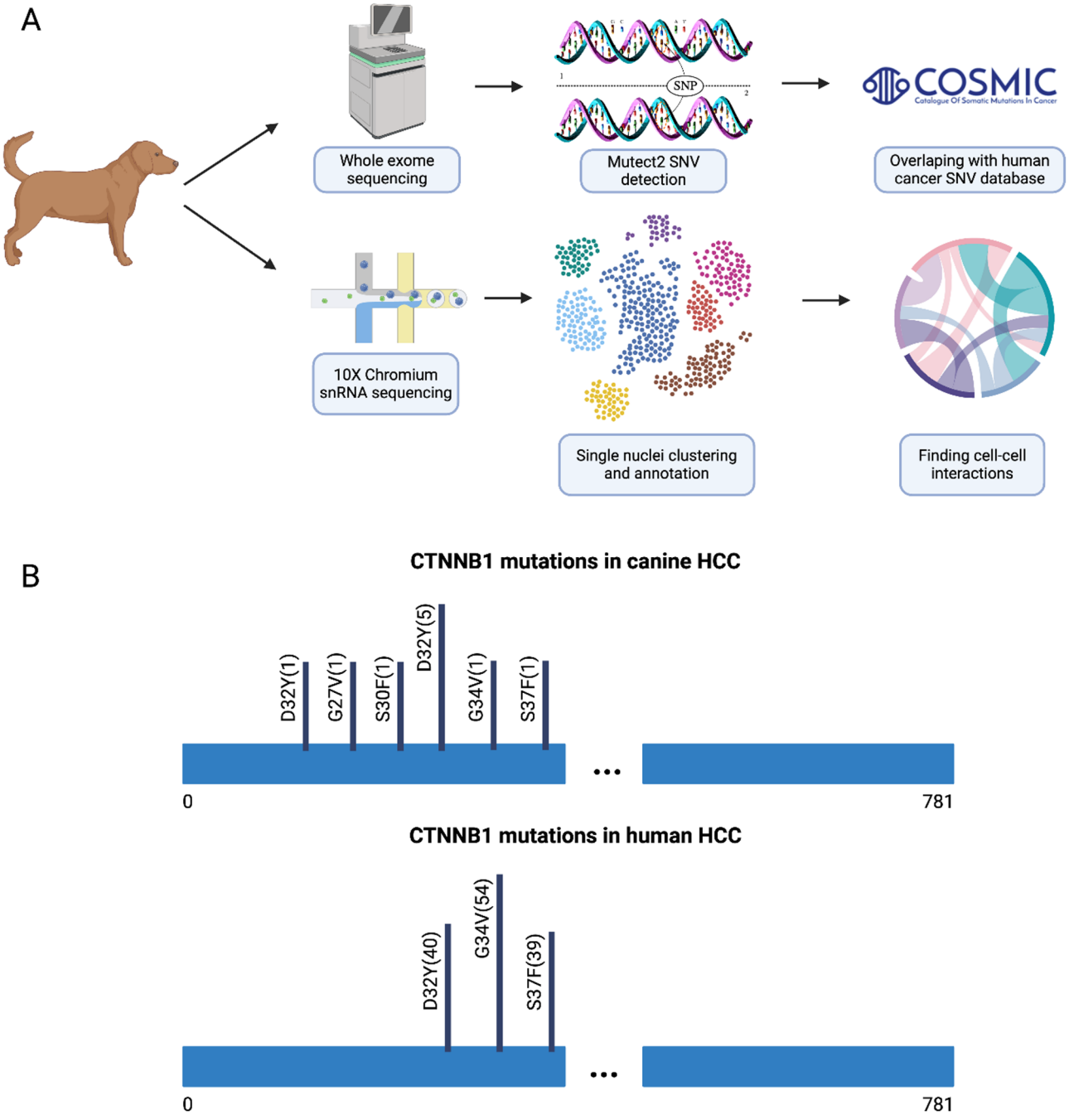

Fig. 1 Study design for multi-omic evaluation of dog HCC. **A** Workflow of sample collection, WES, snRNA-seq, and the primary computational analyses performed. **B** The location and recurrence of *CTNNB1* mutations in dog and human HCC samples. Each mutation is represented as a black bar with the labeled amino acid substitution and its relative protein position. The total number of mutated samples is in parentheses while the height of each bar reflects the number of samples with corresponding SNVs. The blue bar shows the CTNNB1 protein size with gaps denoted as three dots introduced to simplify visualization

board-certified veterinary pathologist at the respective Schools of Veterinary Medicine at University of California-Davis, CA or University of Missouri-Columbia, MO were determined to be HCC. In general, the tumors were expansile and locally infiltrative masses composed of large neoplastic hepatocytes in cellular sheets. Within the mass, there was often multifocal coalescing coagulative necrosis and hemorrhage (Suppl. Fig. 1). Additional clinical information is available for each of the 10 dog samples used for exome sequencing or snRNAseq (Suppl. Table 1).

Exome sequencing

To discover the landscape of somatic missense or loss-of-function protein-coding mutations in HCC we performed WES on a total of 20 samples, 10 HCC tumor and their matched normal blood samples. The sequencing statistics show high-quality WES data across all samples (Suppl. Table 3). Overall, sequence quality was high with sequencing error rates averaging 0.35%. With a sequencing depth across all samples of 100x achieved we show 93.7 to 95.2% of the reads were successfully mapped to the dog reference genome.

HCC somatic mutation discovery

A total of 1,895 non-synonymous SNVs with an average of 189 per sample were identified after filtering, of which 645 mutations with high, moderate, or low impact VEP scores remained. We then focused on the variants with the highest predicted impact, specifically those that truncate proteins through the acquisition of stop codons, splice site shifts, and frameshifts in translation. Most of the mutations were missense (74%), followed by splice region mutations (9%) and frameshift mutations (5%). This WES evaluation of dog HCC shows ten putative driver genes of HCC which occurred in at least 2 (20%) samples (Table 1). The most recurrent missense mutation was in the *CTNNB1* gene in 5 (50%) samples. Notably, this gene is also frequently mutated in human HCC, present in 22% of cases [41]. We analyzed the locations of *CTNNB1* mutations in dog and human genomes, revealing noteworthy similarities (Fig. 1B). Identical D32Y, G34V, and S37F amino acid substitutions were found in both species, appearing in 5, 1, and 1 dog, and in 40, 54, and 39 human samples, respectively. A search of the druggable genes database DGIdb 5.0 shows 66 total *CTNNB1* interactions with 16 FDA approved therapies, suggesting possible treatment alternatives that could be considered after the appropriate validation [56]. The next highest number of affected genes was *ARRDC3* frameshift variants, which were found in three (33%) dog samples (Suppl. Fig. 2). However, no frameshift mutations in *ARRDC3* were observed in human HCC data.

Table 1 Dog genes with high-impact somatic mutations that have previously been identified in human HCC

Gene symbol	% Mutation in dogs	Mutation type	% Mutation in human
CTNNB1	50	Missense	22
ARRDC3	33	Frameshift	0.2
CD93	20	Missense	1.2
CNOT1	20	Missense	3.5
DCTN1	20	Missense	1.1
HIC2	20	Frameshift	0.1
PLCL1	20	Missense	4.1
PYGM	20	Missense	0.9
RBBP4	20	Missense	1.0
SUSD4	20	Missense	2.2

Tumor mutation burden

TMB has been found in humans to be informative for immunotherapy response but its utility in profiling dog tumors is unknown [57, 58]. Since TMB thresholds for defining "high" levels vary by tumor type and are not universally standardized, thus complicating its clinical application, we sought to first compare dog HCC TMB with human data. The median TMB in our cohort of dogs with HCC was 4.01 mutations/Mb (range:2.31–5.96 mutations/Mb) which is similar to the estimated human HCC TMB median range of 2.56 to 5 mutations/Mb (Suppl. Fig. 3) [42–45].

Dog HCC cell type annotation

The processing of all sequenced nuclei, ambient signal filtering, and sample integration resulted in a total of 23,877 nuclei with mean reads detected per nucleus of 1,659. Upon clustering and manual annotation, seven major cell types were identified: fibroblasts, hepatocytes, macrophages, malignant cells, proliferating cells of myeloid origin, endothelial cells, and T cells (Fig. 2A, B). The distribution and intensity of expressed genes that define each cell type are illustrated (Fig. 2B). A UMAP visualization showing the distribution of cell types across individual samples is presented in Supplementary Fig. 4.

Malignant cells were identified through differential expression analysis, revealing genes such as *CP, APOB, DST,* and *PTGR1*, which have been previously reported as overexpressed in malignant cells in human HCC scRNA-seq studies (Suppl. Fig. 5) [59, 60]. To provide additional evidence for the identification of malignant cells, we calculated enrichment scores using a previously defined set of cancer stemness genes for each cell type (Fig. 2C) [54]. A one-tailed t-test comparing the cancer stemness scores between malignant cells and hepatocytes revealed that malignant cells have significantly higher cancer stemness scores than hepatocytes (95% CI: 0.12 to ∞, $p < 2.2 \text{ X } 10\text{-}16$). The high cancer stemness score in proliferating myeloid cells likely results from their progenitor-like properties, which share transcriptional programs with cancer stem cells. In both samples, normal hepatocytes made up most nuclei followed by endothelial and T cells (Fig. 2D). Proliferating myeloid cells and malignant cells demonstrated significantly higher S and G2M phase module scores when compared to other cell types (Suppl. Fig. 6).

We compared the molecular landscape of these dog HCC tumors to a snRNA-seq dataset from two human patients with non-viral HCC [29]. We manually annotated the clusters from the snRNA-seq study of HCC

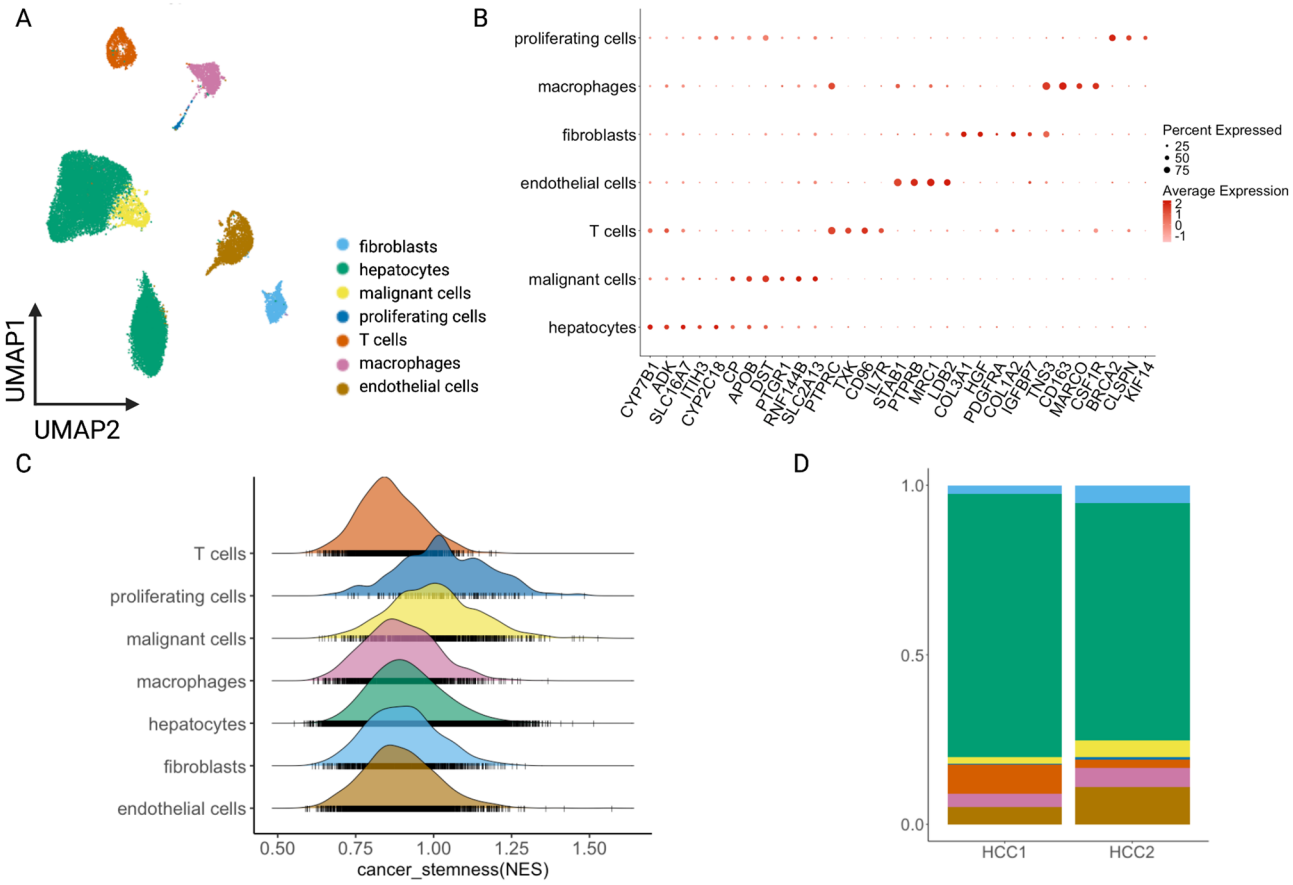

Fig. 2 Dog HCC snRNA-seq data analysis. **A** UMAP visualization of integrated snRNA-seq data from two dogs with annotated cell types. **B** Dotplot of differentially expressed marker genes used for cell type annotation. **C** Enrichment of cancer stemness gene set in clusters. **D** Proportion of cell types in each dog sample

using the cell markers provided in the original paper. The human snRNA-seq dataset included 14,983 nuclei derived from two tumor samples, classified into five major cell types: endothelial cells, macrophages, hepatocytes, fibroblasts, and T cells. Although these samples originated from tumors, Alvarez et al. did not annotate any epithelial cells as malignant. Here, we use "epithelial cells" as an umbrella term encompassing both hepatocytes, which are normal epithelial cells of the liver, and malignant cells. To enable comparison with our dog data, we contrasted epithelial cells from tumor samples with those from adjacent normal tissues and identified a cluster exclusive to tumor samples, which we annotated as malignant cells.

To compare the TME compositions of dog and human HCC snRNA-seq data, we fully integrated the data sets of both species. Overall, we showed that non-epithelial cells from the two species integrated more effectively than epithelial cells (Fig. 3A, B). T cells, macrophages, fibroblasts, and endothelial cells formed shared clusters corresponding to their cell types, whereas hepatocytes remained largely species-specific. Dog malignant and proliferating cells did not integrate with human epithelial cells, indicating strong species specificity (Fig. 3B).

To evaluate similarities in cell type gene expression signatures, we defined the size of the intersection of the sets divided by the size of their union, a Jaccard similarity index (Suppl. Fig. 7). Human endothelial cells exhibited high index values for both dog endothelial cells and fibroblasts, while human macrophages were most similar to dog macrophages and T cells. Discrepancies between species were observed in hepatocytes, malignant cells, and proliferating cells, which aligns with our findings from the integrated clustering (Fig. 3B).

Next, we used an approach that compares transcriptional programs across species [61]. Specifically, we performed differential gene expression analysis between pairs of cell types (e.g., macrophages vs. T cells) within each species and then compared the resulting transcriptional signatures between species to identify conserved and species-specific genes. When comparing representative innate and adaptive lineages, macrophages and T cells, we observed an overlap in gene expression patterns with well-established macrophage gene markers such as

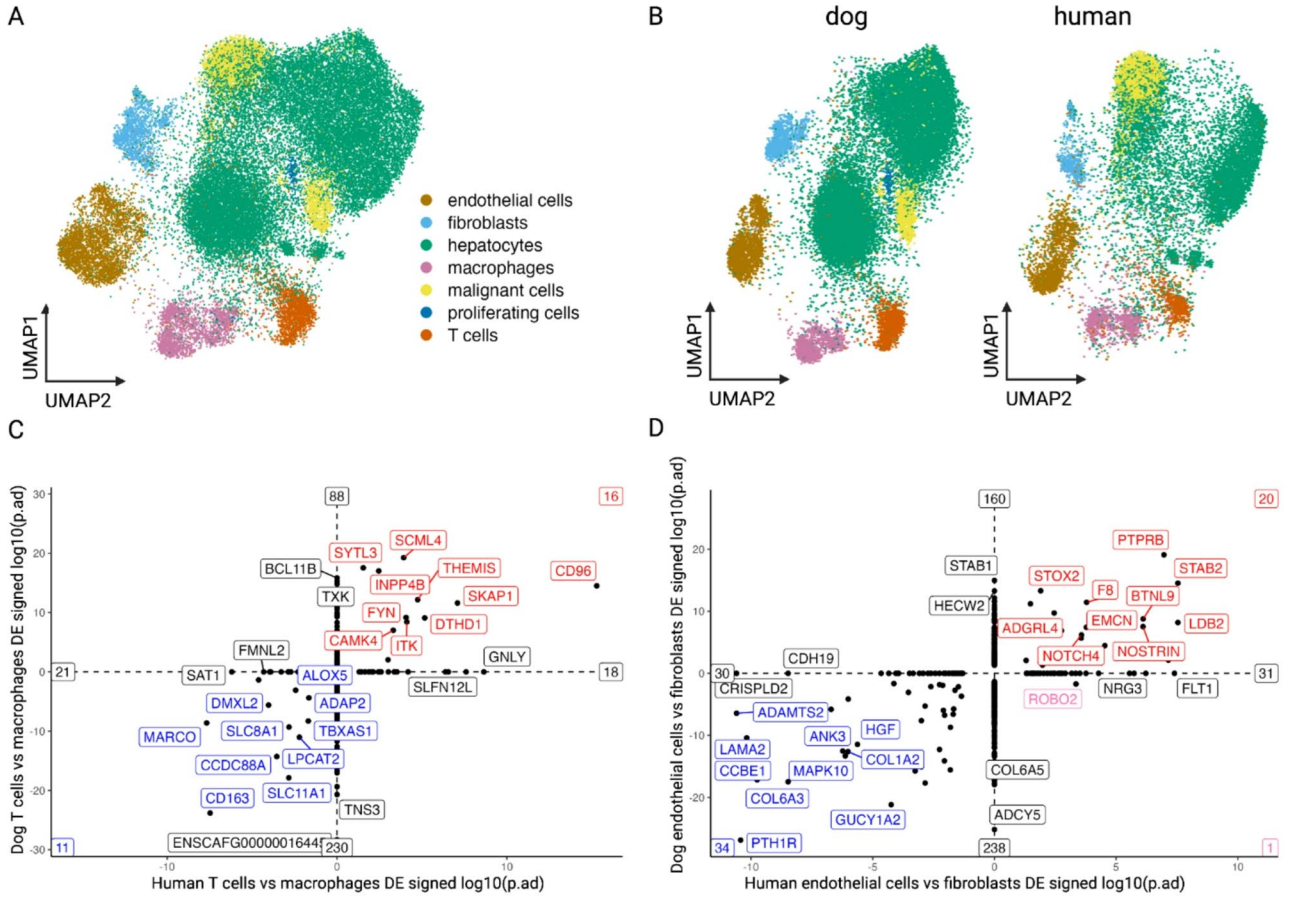

Fig. 3 A tumor microenvironment comparison between dog and human HCC. **A** UMAP visualization of cell types for integrated dog and human samples. **B** UMAP visualization of cell types separated for dog and human. In panels **C** and **D**, specific intercellular comparisons show significantly upregulated (red) and downregulated (blue) features in the top-right and bottom-left quadrants, respectively are depicted with sign log10 adjusted *p*-values. Conflicting features (pink) and species-specific features (black) are labeled. The red or blue numbers in the upper right or lower left quadrants at the ends of the axis lines represent how many features fell in that quadrant

MARCO and *CD163* enriched in both species (Fig. 3C). The most highly conserved gene features in T cells included a cell surface marker CD96 along with some intracellular proteins such as *SKAP1, SCML4, THEMIS, ITK, CAMK4*, and *FYN* which are associated with various T cell functions (Fig. 3C). Interesting discrepancies included the gene expression of *BCL11B* and *TXK* as defining features in dog T cells but nonsignificant in human T cells. Additionally, *GNLY* was highly expressed in human T cells but was not significantly expressed in dog samples. When comparing endothelial cells to fibroblasts, we observed that endothelial markers such as *PTPRB, STAB2, STOX2,* and *F8* were conserved across species, whereas *STAB1* was specific to dog samples. For fibroblasts, the shared markers included *PTH1R, COL6A3,* and *COL1A2,* whereas *COL6A5* was exclusively expressed in dog fibroblasts (Fig. 3D). In summary, our analysis shows that human and dog HCC cell types share highly consistent gene signatures.

HCC cell-to-cell communication

Advantageous cellular crosstalk is vital to tumor survival, whether through the development of chemoresistance or the escape of immune surveillance [62]. We evaluated the inferred HCC cell-cell interactions within dog and human TMEs using CellPhoneDB [55]. Analysis revealed that the dog and human HCC had 222 and 227 ligand-receptor pairs in total, respectively (Suppl. Fig. 8). In the seven major cell types (Fig. 2A) evaluated in the dog samples, we identified significant interactions ($p < 0.05$) across 36 signaling pathways. The number of interactions and the predicted interaction strength of incoming versus outgoing signals were used to infer the activity of cells within each species' TME (Fig. 4). The top three cell types predicted to have the strongest interactions in dogs were fibroblasts, endothelial, and malignant cells. Similarly, in human HCC, 35 significant interactions were associated with independent signaling pathways, with malignant cells displaying the greatest number of interactions while fibroblasts, endothelial, and malignant cells exhibited the

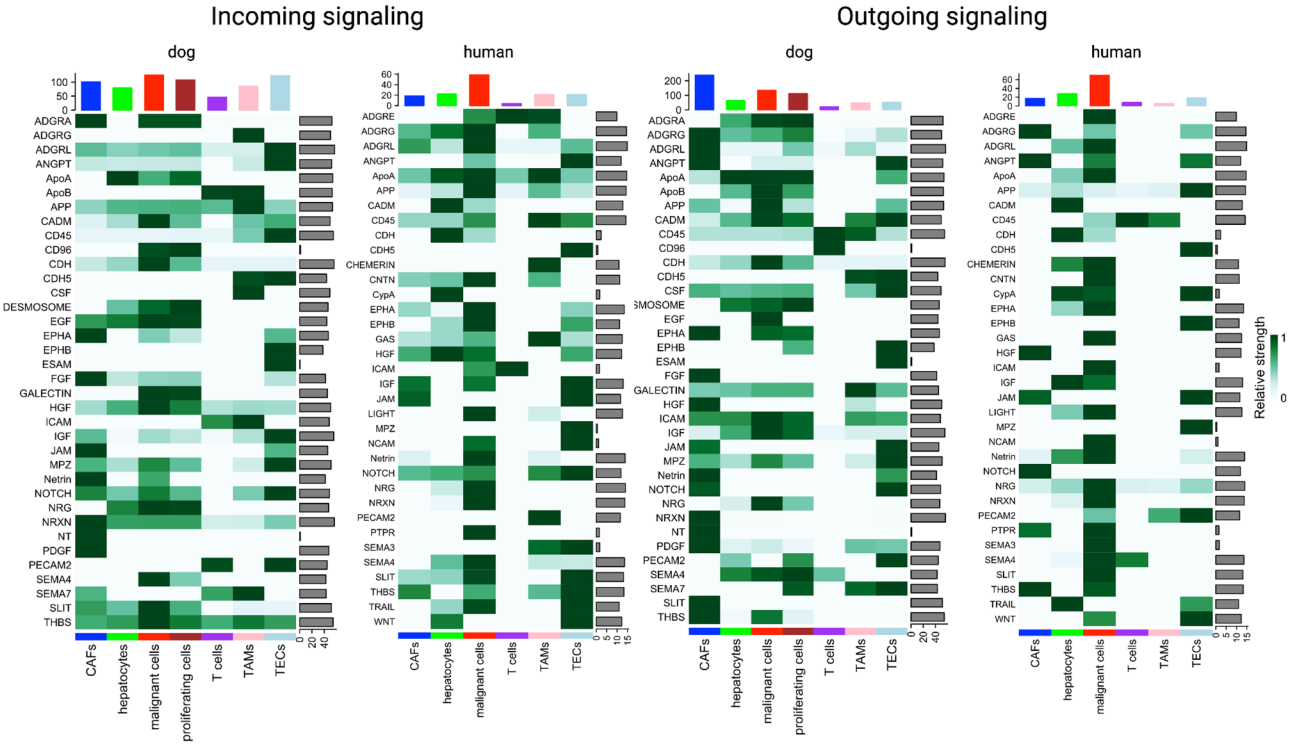

Fig. 4 Heatmaps of incoming and outgoing pathway signaling in dog and human snRNA-seq datasets. The color bar intensity (0 to 1 scale) represents the relative signaling strength of an expressed gene across cell types. The grey side bars indicate the sum of the signaling strength of each cell type or pathway

strongest incoming and outgoing interactions. Figure 4 shows that human malignant cells (red bar on the right) were more involved in ligand receptor interactions with immune and stromal cells than dog malignant cells (red bar on the left). In humans, malignant cells participated in pathways such as *ADGRE, ADGRL, Chemerin, CNTN, CypA, GAS, LIGHT,* and *NCAM*, while in dogs, interactions were more focused on fibroblasts. Pathways involving TECs, CAFs, and T cells, including *HGF, ICAM, IGF, JAM, NOTCH,* and *THBS*, were shared between both species. This supports our earlier finding that immune and stromal compartments are more conserved across species, while malignant cells differ.

Next, we analyzed ligand-receptor interactions within each pathway and compared them between species. Our goal was to identify both species-specific and shared interactions in the HCC TME, focusing on distinct and overlapping signaling pathways in each species. In dog tumors, we identified several pathways not seen in human data, including *ADGRA, CADM, CSF, DESMOSOME, EGF, FGF, GALECTIN, MPZ*, and *PDGF*. Within these, two interactions stood out as unique to dog HCC: *IL34–CSF1R* and *LGALS9–P4HB* (Fig. 5A). In contrast, human specific interactions included *Chemerin–CMKLR1* and two interactions involving *GAS6* and *TAM* family receptors *Tyro3, Axl,* and *MerTK* (Fig. 5C). As shared interactions were mainly found between stromal or immune cells and malignant cells, we further examined these pathways. We identified several key shared interactions between malignant cells and fibroblasts, including *IGF1–IGF1R, ANGPT1–TEK, JAG1–NOTCH2, THBS1*/*THBS2–CD36,* and *APP–SORL*. Shared interactions between macrophages and malignant cells, such as *PTPRC–MRC1, THBS1–CD36,* and *APP–CD74*, highlighted conserved cellular communication networks in both species (Fig. 5B, D). Together, these analyses reveal both conserved and species specific patterns of cell communication in HCC. While shared interactions reflect fundamental features of TME organization in both species, species-specific interactions may represent divergent mechanisms of tumor progression or immune regulation that could become relevant for therapeutic discovery as more data and functional validation studies emerge.

Discussion

In this study, we conducted an integrative analysis of dog HCC by combining WES and snRNA sequencing to gain new comparative insights into the molecular and cellular features of the TME. Analysis of WES data identified recurrent mutations in the *CTNNB1* gene in five out of ten HCC samples. Notably, *CTNNB1* is one of the most frequently mutated genes in human HCC, and its relevance in dogs is underscored by its role in encoding

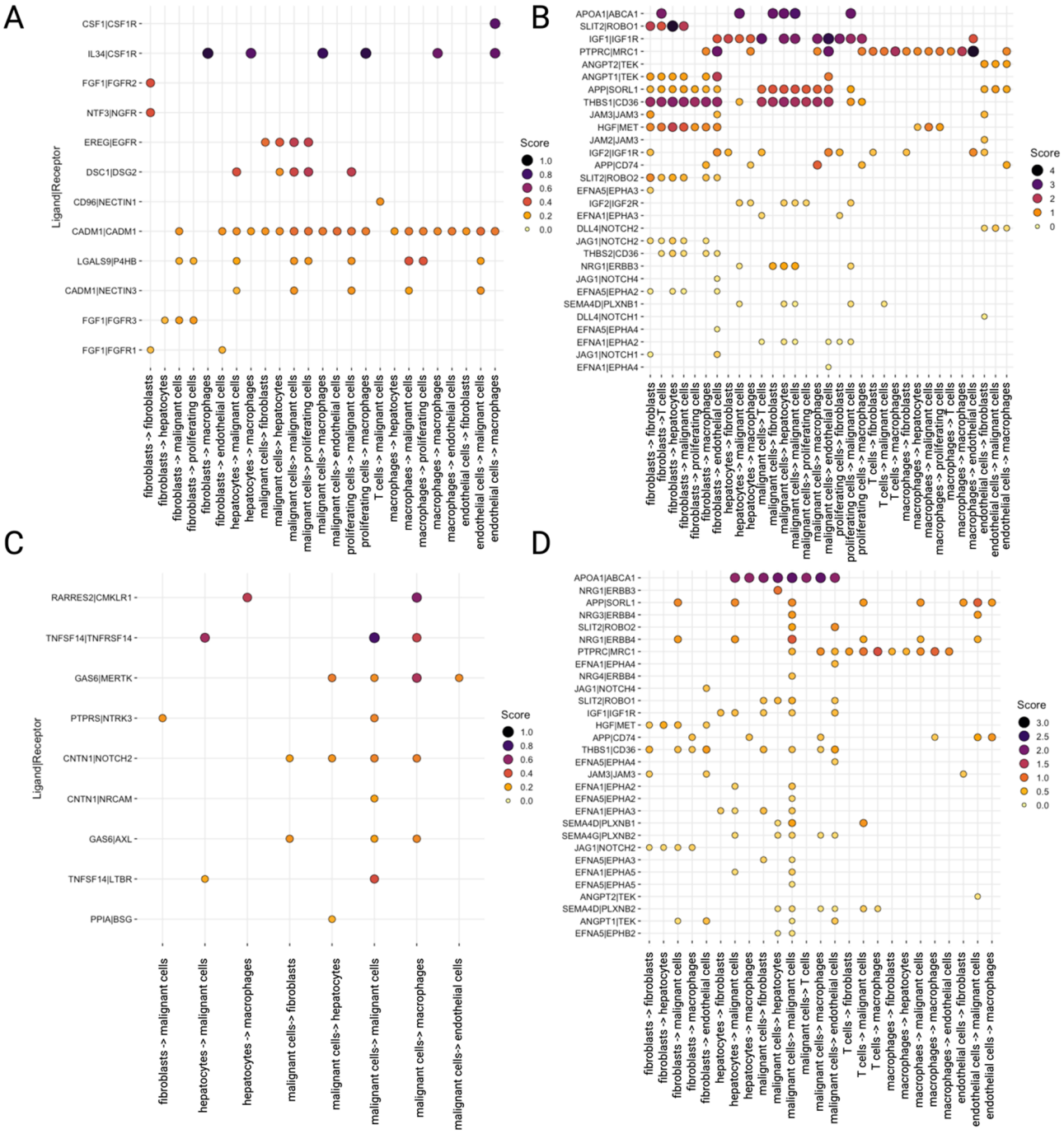

Fig. 5 Cell-cell interactions between malignant and immune cells. The x-axis indicates the cell types expressing ligands and receptors, while the y-axis denotes the corresponding ligand–receptor pairs. Interaction scores, computed using CellPhoneDB, represent the mean expression levels of each ligand–receptor pair within the respective cell types. **A** Interactions derived from pathways identified as unique to dog samples. **B** Interactions from conserved pathways detected in dog snRNA-seq data. **C** Interactions derived from pathways identified as unique to human samples. **D** Interactions from conserved pathways detected in human snRNA-seq data

-catenin, a central component of the Wnt beta β-catenin signaling pathway. This pathway plays a key role in liver cancer development, tumor progression, and immune evasion [63–65]. While our dog cohort is relatively small, the shared presence of *CTNNB1* mutations suggests similar oncogenic mechanisms between dog and human HCC. However, -catenin has long been considered a difficult therapeutic target due to its lack of deep binding pockets and extensive domain overlap with other proteins such as *TCF* and *LEF* transcription factors [66].

Currently, *CTNNB1*-targeted therapies for liver cancer are not yet clinically established in humans, but several experimental strategies and investigational drugs are being developed to exploit this pathway. The outcome of these druggable gene trials could inform future treatment options for dog HCC should a larger study cohort confirm the importance of this pathway.

Our comparative analysis of the HCC tumor biology shows comparable transcriptional programs in immune and stromal cell types between humans and dogs, whose functional relevance remains unclear. This conservation likely reflects shared evolutionary pressures on immune surveillance and stromal maintenance, as these functions are critical across mammalian species [14, 16]. However, malignant and epithelial cell populations displayed more pronounced species-specific differences, potentially driven by variation in tissue homeostasis, regenerative capacity, mutational landscapes, and tumor evolutionary trajectories between humans and dogs [8, 17]. Species-specific patterns of epithelial biology and oncogenic transformation likely contribute to the observed transcriptional differences, especially in highly heterogeneous tumors like HCC. Together, these results highlight both the promise and the challenges of cross-species modeling: while conserved immune and stromal programs make dogs valuable translational models for studying tumor-immune interactions, species-specific differences in malignant and epithelial cells underscore the need for cautious interpretation when extrapolating findings to human cancers.

In both human and dog HCC, through inference we identified shared ligand-receptor interactions that reflect known drivers of tumor progression, such as *IGF1-IGF1R, ANGPT1-TEK, JAG1-NOTCH,* and *Thrombospondin-1-CD36*, all linked to cancer stemness, angiogenesis, and immune evasion [67–74]. Species-specific interactions were also detected in dogs, including *IL34-CSF1R* and *LGALS9-P4HB*, both associated with macrophage regulation and tumor-driven immunosuppression, suggesting potential therapeutic targets [75–78]. In human HCC, unique interactions such as *Chemerin-CMKLR1* and *GAS6-MerTK/Axl* were identified, both known to promote tumor progression [79–82]. The observed cellular crosstalk includes both conserved and species-specific ligand–receptor interactions in spontaneous HCC, offering new insights that can advance our understanding of human liver cancer.

While these comparisons offer important insights, it is worth noting certain technical limitations of single nuclei evaluations that can influence the interpretation of the cellular landscape. A common approach in human tumor scRNA-seq studies is to use inferred copy number variation (CNV) to help distinguish malignant from non-malignant cells. However, in our dog snRNA-seq dataset, CNV inference was limited by lower resolution, high dropout rates, and the lack of a high-quality normal liver reference in dogs. These constraints likely contribute to the observed clustering proximity seen between malignant and hepatocyte clusters in dog HCC, which limits the generalizability of some malignant cell biology.

Despite its preliminary nature, this study represents the first integrated analysis of potential genetic drivers in canine HCC, while also advancing our understanding of the TME and providing foundational insights into its molecular and cellular features. These findings lay the groundwork for future multiomic studies in larger canine cohorts and offer a valuable resource for comparative oncology. Our results support cross-species hypothesis generation that can inform the identification of therapeutic targets to test in dogs and resistance mechanisms relevant to both human and veterinary liver cancer research.

Supplementary Information

The online version contains supplementary material available at https://doi.org/10.1186/s44356-025-00037-0.

Supplementary Material 1.

Supplementary Material 2: Supplementary Figure 1. Hematoxylin and eosin-stained images of cross sectioned dog HCC tumors. Left panel: The tumor consisted of broad trabeculae and sheets of neoplastic cells with irregularly dilated blood vessels and multifocal hemorrhage. Bar = 500um resolution. Right panel: The tumor cells were arranged in broad cellular trabeculae that were often 4 or 5-cells thick. The tumor cells exhibited mild to moderate anisokaryosis and anisocytosis. Bar = 20um resolution. Supplementary Figure 2. Frameshift somatic mutations present in the ***ARRDC3*** gene for three individual dogs with HCC. Supplementary Figure 3. Boxplots of TMB values with median lines. The dark purple box values were computed for our dog cohort, while the other data were sourced from different HCC cohorts (18,94–96). Supplementary Figure 4. Visualization of nuclei from each dog HCC sample in integrated data. Supplementary Figure 5. Differentially expressed gene patterns in dog malignant cells visualized on human HCC data (see methods for sources). Supplementary Figure 6. UMAP visualization of cell cycle scores in dog HCC snRNA-seq data. G2M (left panel) and S (right panel) module scores were assigned based on average expression of their respective cell cycle genes. Supplementary Figure 7. Heatmap illustrating the Jaccard similarity index, measuring the overlap between dog cell type gene signatures (rows) and human cell type gene signatures (columns). Supplementary Figure 8. A cross-species heatmap classification of estimated cell to cell interaction numbers per cell type pairing. Left and right panels are the CellPhoneDB analyses of dog and human HCC snRNAseq data, respectively. We show the appropriate color scale range for each.

Authors' contributions

Conception and design: W.C.W., Y.I.N. Experimentation and data acquisition: A.K., J.N.B., K.M., H.A., E.S.R. Data analysis and manuscript drafting: W.C.W., Y.I.N., S.T.K. Final approval of completed manuscript: All authors.

Funding

This study was supported by the University of Missouri internal funds.

Data availability

Raw whole exome sequencing data for ten dog HCC samples is available in the NCBI database under accession number PRJNA1237364. Additionally, both raw and processed single-nucleus RNA sequencing (snRNA-seq) data from two HCC dogs can be accessed in the NCBI GEO database under accession number GSE292303. Human snRNA-seq data is available in the NCBI GEO under accession number GSE189175.

Declarations

Ethics approval and consent to participate

All tumor and normal blood samples were obtained under studies approved by the University of California, Davis or University of Missouri Institutional Animal Care and Use Committees. We complied with all relevant ethical regulations for animal use and all dog owners provided informed consent prior to sample collection.

Competing interests

The authors declare no competing interests.

Author details

[1]Institute of Data Science and Informatics, University of Missouri, Columbia, MO, USA
[2]Department of Veterinary Medicine and Surgery, College of Veterinary Medicine, University of Missouri, Columbia, MO, USA
[3]College of Biological Sciences, University of Minnesota, Minneapolis, MN, USA
[4]Department of Surgical and Radiological Sciences, School of Veterinary Medicine, Davis, CA, USA
[5]Broad Institute of MIT and Harvard, Cambridge, MA, USA
[6]Bioinformatics and Analytics Core, University of Missouri, Columbia, MO, USA
[7]Division of Animal Sciences, University of Missouri, Columbia, MO, USA
[8]Palaeogenomics Group, Institute of Palaeoanatomy, Domestication Research and the History of Veterinary Medicine, Ludwig-Maximilians-Universität, Munich, Germany
[9]Department of Colon and Rectal Surgery, Lerner Research Institute, Cleveland Clinic Foundation, Cleveland, OH, USA
[10]Department of Surgery, School of Medicine, University of Missouri, Columbia, MO, USA
[11]Department of Surgery and Immunology, UConn Health School of Medicine, Farmington, CT, USA

Received: 25 March 2025 / Accepted: 4 August 2025
Published online: 23 October 2025

References

1. Llovet JM, Kelley RK, Villanueva A, Singal AG, Pikarsky E, Roayaie S, et al. Hepatocellular carcinoma. Nat Rev Dis Primers. 2021;7(1): 6.
2. Samant H, Amiri HS, Zibari GB. Addressing the worldwide hepatocellular carcinoma: epidemiology, prevention and management. J Gastrointest Oncol. 2021;12(Suppl 2):S361-73.
3. Llovet JM, Castet F, Heikenwalder M, Maini MK, Mazzaferro V, Pinato DJ, et al. Immunotherapies for hepatocellular carcinoma. Nat Rev Clin Oncol. 2022;19(3):151–72.
4. Finn RS, Qin S, Ikeda M, Galle PR, Ducreux M, Kim TY, et al. Atezolizumab plus bevacizumab in unresectable hepatocellular carcinoma. N Engl J Med. 2020;382(20):1894–905.
5. Ren Z, Xu J, Bai Y, Xu A, Cang S, Du C, et al. Sintilimab plus a bevacizumab biosimilar (IBI305) versus sorafenib in unresectable hepatocellular carcinoma (ORIENT-32): a randomised, open-label, phase 2–3 study. Lancet Oncol. 2021;22(7):977–90.
6. Wang Z, Wang Y, Gao P, Ding J. Immune checkpoint inhibitor resistance in hepatocellular carcinoma. Cancer Lett. 2023;555(216038): 216038.
7. Manfredi GF, Celsa C, John C, Jones C, Acuti N, Scheiner B, et al. Mechanisms of resistance to immunotherapy in hepatocellular carcinoma. J Hepatocell Carcinoma. 2023;10:1955–71.
8. LeBlanc AK, Mazcko CN. Improving human cancer therapy through the evaluation of pet dogs. Nat Rev Cancer. 2020;20(12):727–42.
9. Mannheimer JD, Tawa G, Gerhold D, Braisted J, Sayers CM, McEachron TA, et al. Transcriptional profiling of canine osteosarcoma identifies prognostic gene expression signatures with translational value for humans. Commun Biol. 2023;6(1): 856.
10. Dow S. A role for dogs in advancing cancer immunotherapy research. Front Immunol. 2019;10: 2935.
11. LeBlanc A, Mazcko CN, Mason NJ, Chambers MR, Brockington DM, Pluhar GE, et al. Comparative oncology in action: vignettes on immunotherapy development. Vet Oncol. 2025;2(1): 5.
12. LeBlanc AK, Mazcko C, Brown DE, Koehler JW, Miller AD, Miller CR, et al. Creation of an NCI comparative brain tumor consortium: informing the translation of new knowledge from canine to human brain tumor patients. Neuro Oncol. 2016;18(9):1209–18.
13. Patkar S, Mannheimer J, Harmon S, Mazcko C, Choyke P, Brown GT, et al. Large Scale Comparative Deconvolution Analysis of the Canine and Human Osteosarcoma Tumor Microenvironment Uncovers Conserved Clinically Relevant Subtypes. bioRxivorg. 2023;2023(09.27):559797.
14. Ammons DT, Hopkins LS, Cronise KE, Kurihara J, Regan DP, Dow S. Single-cell RNA sequencing reveals the cellular and molecular heterogeneity of treatment-naïve primary osteosarcoma in dogs. Commun Biol. 2024;7(1): 496.
15. Ammons DT, Harris RA, Hopkins LS, Kurihara J, Weishaar K, Dow S. A single-cell RNA sequencing atlas of circulating leukocytes from healthy and osteosarcoma affected dogs. Front Immunol. 2023. https://doi.org/10.3389/fimmu.2023.1162700.
16. Garden OA, Volk SW, Mason NJ, Perry JA. Companion animals in comparative oncology: one medicine in action. Vet J. 2018;240:6–13.
17. Gardner HL, Fenger JM, London CA. Dogs as a model for cancer. Annu Rev Anim Biosci. 2016;4:199–222.
18. Wahida A, Buschhorn L, Fröhling S, Jost PJ, Schneeweiss A, Lichter P, et al. The coming decade in precision oncology: six riddles. Nat Rev Cancer. 2023;23(1):43–54.
19. Wu K, Rodrigues L, Post G, Harvey G, White M, Miller A, et al. Analyses of canine cancer mutations and treatment outcomes using real-world clinico-genomics data of 2119 dogs. NPJ Precis Oncol. 2023;7(1):1–8.
20. Anderson EC, DiPalazzo J, Lucas FL, Hall MJ, Antov A, Helbig P, et al. Genome-matched treatments and patient outcomes in the Maine cancer genomics initiative (MCGI). NPJ Precis Oncol. 2024;8(1): 67.
21. Rodrigues L, Watson J, Feng Y, Lewis B, Harvey G, Post G, et al. Shared hotspot mutations in oncogenes position dogs as an unparalleled comparative model for precision therapeutics. Sci Rep. 2023;13(1): 10935.
22. Sakthikumar S, Warrier M, Whitley D, Facista S, Adkins J, Aman S, et al. Genomic analysis across 53 canine cancer types reveals novel mutations and high clinical actionability potential. Vet Comp Oncol. 2024;22(1):30–41.
23. Mereu E, Lafzi A, Moutinho C, Ziegenhain C, McCarthy DJ, Álvarez-Varela A, et al. Benchmarking single-cell RNA-sequencing protocols for cell atlas projects. Nat Biotechnol. 2020;38(6):747–55.
24. Zhang M, Yang H, Wan L, Wang Z, Wang H, Ge C, et al. Single-cell transcriptomic architecture and intercellular crosstalk of human intrahepatic cholangiocarcinoma. J Hepatol. 2020;73(5):1118–30.
25. Xie Z, Huang J, Li Y, Zhu Q, Huang X, Chen J, et al. Single-cell RNA sequencing revealed potential targets for immunotherapy studies in hepatocellular carcinoma. Sci Rep. 2023;13(1): 18799.
26. Lu Y, Yang A, Quan C, Pan Y, Zhang H, Li Y, et al. A single-cell atlas of the multicellular ecosystem of primary and metastatic hepatocellular carcinoma. Nat Commun. 2022;13(1): 4594.
27. Zheng C, Zheng L, Yoo JK, Guo H, Zhang Y, Guo X, et al. Landscape of infiltrating T cells in liver cancer revealed by Single-Cell sequencing. Cell. 2017;169(7):1342–e5616.
28. Sun Y, Wu L, Zhong Y, Zhou K, Hou Y, Wang Z, et al. Single-cell landscape of the ecosystem in early-relapse hepatocellular carcinoma. Cell. 2021;184(2):404–e2116.
29. Alvarez M, Benhammou JN, Darci-Maher N, French SW, Han SB, Sinsheimer JS, et al. Human liver single nucleus and single cell RNA sequencing identify a hepatocellular carcinoma-associated cell-type affecting survival. Genome Med. 2022;14: 50.
30. Qu X, Zhao X, Lin K, Wang N, Li X, Li S, et al. M2-like tumor-associated macrophage-related biomarkers to construct a novel prognostic signature, reveal the immune landscape, and screen drugs in hepatocellular carcinoma. Front Immunol. 2022;13:994019.
31. Yu L, Shen N, Shi Y, Shi X, Fu X, Li S, et al. Characterization of cancer-related fibroblasts (CAF) in hepatocellular carcinoma and construction of CAF-based risk signature based on single-cell RNA-seq and bulk RNA-seq data. Front Immunol. 2022;13: 1009789.
32. Hao X, Zheng Z, Liu H, Zhang Y, Kang J, Kong X, et al. Inhibition of APOC1 promotes the transformation of M2 into M1 macrophages via the ferroptosis pathway and enhances anti-PD1 immunotherapy in hepatocellular carcinoma based on single-cell RNA sequencing. Redox Biol. 2022;56: 102463.
33. Xiong Z, Chan SL, Zhou J, Vong JSL, Kwong TT, Zeng X, et al. Targeting PPAR-gamma counteracts tumour adaptation to immune-checkpoint blockade in hepatocellular carcinoma. Gut. 2023;72(9):1758–73.

34. Santos NP, Colaço AA, Oliveira PA. Animal models as a tool in hepatocellular carcinoma research: a review. Tumour Biol. 2017;39(3): 1010428317695923.
35. Moyer J, Lopez DJ, Balkman CE, Sumner JP. Factors associated with survival in dogs with a histopathological diagnosis of hepatocellular carcinoma: 94 cases (2007–2018). Open Vet J. 2021;11(1):144–53.
36. Wang C, Wallerman O, Arendt ML, Sundström E, Karlsson Å, Nordin J, et al. A novel canine reference genome resolves genomic architecture and uncovers transcript complexity. Commun Biol. 2021;4: 185.
37. Kim D, Paggi JM, Park C, Bennett C, Salzberg SL. Graph-based genome alignment and genotyping with HISAT2 and HISAT-genotype. Nat Biotechnol. 2019;37(8):907–15.
38. McKenna A, Hanna M, Banks E, Sivachenko A, Cibulskis K, Kernytsky A, et al. The genome analysis toolkit: a mapreduce framework for analyzing next-generation DNA sequencing data. Genome Res. 2010;20(9):1297–303.
39. McLaren W, Gil L, Hunt SE, Riat HS, Ritchie GRS, Thormann A, et al. The ensembl variant effect predictor. Genome Biol. 2016;17(1): 122.
40. Merino DM, McShane LM, Fabrizio D, Funari V, Chen SJ, White JR, et al. Establishing guidelines to harmonize tumor mutational burden (TMB): in silico assessment of variation in TMB quantification across diagnostic platforms: phase I of the friends of cancer research TMB harmonization project. J Immunother Cancer. 2020;8(1): e000147.
41. Tate JG, Bamford S, Jubb HC, Sondka Z, Beare DM, Bindal N, et al. COSMIC: the catalogue of somatic mutations in cancer. Nucleic Acids Res. 2019;47(Database issue):D941.
42. Cowzer D, White JB, Chou JF, Chen PJ, Kim TH, Khalil DN, et al. Targeted molecular profiling of Circulating Cell-Free DNA in patients with advanced hepatocellular carcinoma. JCO Precis Oncol. 2023;7:e2300272.
43. Schulze K, Imbeaud S, Letouzé E, Alexandrov LB, Calderaro J, Rebouissou S, et al. Exome sequencing of hepatocellular carcinomas identifies new mutational signatures and potential therapeutic targets. Nat Genet. 2015;47(5):505–11.
44. Ng CKY, Dazert E, Boldanova T, Coto-Llerena M, Nuciforo S, Ercan C, et al. Integrative proteogenomic characterization of hepatocellular carcinoma across etiologies and stages. Nat Commun. 2022;13(1): 2436.
45. Harding JJ, Nandakumar S, Armenia J, Khalil DN, Albano M, Ly M, et al. Prospective genotyping of hepatocellular carcinoma: clinical implications of next-generation sequencing for matching patients to targeted and immune therapies. Clin Cancer Res. 2019;25(7):2116–26.
46. Hao Y, Hao S, Andersen-Nissen E, Mauck WM, Zheng S, Butler A, et al. Integrated analysis of multimodal single-cell data. Cell. 2021;184(13):3573–e8729.
47. Zheng GXY, Terry JM, Belgrader P, Ryvkin P, Bent ZW, Wilson R, et al. Massively parallel digital transcriptional profiling of single cells. Nat Commun. 2017;8(1): 14049.
48. Stuart T, Butler A, Hoffman P, Hafemeister C, Papalexi E, Mauck WM, et al. Comprehensive integration of Single-Cell data. Cell. 2019;177(7):1888–e90221.
49. Hafemeister C, Satija R. Normalization and variance stabilization of single-cell RNA-seq data using regularized negative binomial regression. Genome Biol. 2019;20: 296.
50. Zappia L, Oshlack A. Clustering trees: a visualization for evaluating clusterings at multiple resolutions. Gigascience. 2018;7(7): giy083.
51. Franzén O, Gan LM, Björkegren JLM. PanglaoDB: a web server for exploration of mouse and human single-cell RNA sequencing data. Database (Oxford). 2019;2019:baz046.
52. Han Y, Wang Y, Dong X, Sun D, Liu Z, Yue J, et al. TISCH2: expanded datasets and new tools for single-cell transcriptome analyses of the tumor microenvironment. Nucleic Acids Res. 2023;51(D1):D1425–31.
53. Lopez R, Regier J, Cole MB, Jordan MI, Yosef N. Deep generative modeling for single-cell transcriptomics. Nat Methods. 2018;15(12):1053–8.
54. Miranda A, Hamilton PT, Zhang AW, Pattnaik S, Becht E, Mezheyeuski A, et al. Cancer stemness, intratumoral heterogeneity, and immune response across cancers. Proc Natl Acad Sci U S A. 2019;116(18):9020–9.
55. Efremova M, Vento-Tormo M, Teichmann SA, Vento-Tormo R. CellPhoneDB: inferring cell–cell communication from combined expression of multi-subunit ligand–receptor complexes. Nat Protoc. 2020;15(4):1484–506.
56. Cannon M, Stevenson J, Stahl K, Basu R, Coffman A, Kiwala S, et al. DGIdb 5.0: rebuilding the drug-gene interaction database for precision medicine and drug discovery platforms. Nucleic Acids Res. 2024;52(D1):D1227–35.
57. Aggarwal C, Ben-Shachar R, Gao Y, Hyun SW, Rivers Z, Epstein C, et al. Assessment of tumor mutational burden and outcomes in patients with diverse advanced cancers treated with immunotherapy. JAMA Netw Open. 2023;6(5): e2311181.
58. Niknafs N, Balan A, Cherry C, Hummelink K, Monkhorst K, Shao XM, et al. Persistent mutation burden drives sustained anti-tumor immune responses. Nat Med. 2023;29(2):440–9.
59. Meng Y, Zhao Q, An L, Jiao S, Li R, Sang Y, et al. A TNFR2-hnRNPK axis promotes primary liver cancer development via activation of YAP signaling in hepatic progenitor cells. Cancer Res. 2021;81(11):3036–50.
60. Su X, Zhao L, Shi Y, Zhang R, Long Q, Bai S, et al. Clonal evolution in liver cancer at single-cell and single-variant resolution. J Hematol Oncol. 2021;14(1): 22.
61. Pombo Antunes AR, Scheyltjens I, Lodi F, Messiaen J, Antoranz A, Duerinck J, et al. Single-cell profiling of myeloid cells in glioblastoma across species and disease stage reveals macrophage competition and specialization. Nat Neurosci. 2021;24(4):595–610.
62. Armingol E, Officer A, Harismendy O, Lewis NE. Deciphering cell–cell interactions and communication from gene expression. Nat Rev Genet. 2021;22(2):71–88.
63. Xu C, Xu Z, Zhang Y, Evert M, Calvisi DF, Chen X. β-catenin signaling in hepatocellular carcinoma. J Clin Invest. 2022;132(4): e154515.
64. Nakagawa S, Yamaguchi K, Takane K, Tabata S, Ikenoue T, Furukawa Y. Wnt/β-catenin signaling regulates amino acid metabolism through the suppression of CEBPA and FOXA1 in liver cancer cells. Commun Biol. 2024;7(1): 510.
65. Gajos-Michniewicz A, Czyz M. WNT/β-catenin signaling in hepatocellular carcinoma: the aberrant activation, pathogenic roles, and therapeutic opportunities. Genes Dis. 2024;11(2):727–46.
66. Vilchez V, Turcios L, Marti F, Gedaly R. Targeting Wnt/β-catenin pathway in hepatocellular carcinoma treatment. World J Gastroenterol. 2016;22(2):823.
67. Ngo MHT, Jeng HY, Kuo YC, Nanda JD, Brahmadhi A, Ling TY, et al. The role of IGF/IGF-1R signaling in hepatocellular carcinomas: stemness-related properties and drug resistance. Int J Mol Sci. 2021;22(4): 1931.
68. Kiss EA, Saharinen P. Anti-angiogenic Targets: Angiopoietin and Angiopoietin Receptors. Tumor Angiogenesis. 2019;5:227–50.
69. Saharinen P, Eklund L, Alitalo K. Therapeutic targeting of the angiopoietin–TIE pathway. Nat Rev Drug Discov. 2017;16(9):635–61.
70. Leong A, Kim M. The angiopoietin-2 and TIE pathway as a therapeutic target for enhancing antiangiogenic therapy and immunotherapy in patients with advanced cancer. Int J Mol Sci. 2020;21(22): 8689.
71. Giovannini C, Fornari F, Piscaglia F, Gramantieri L. Notch signaling regulation in HCC: from hepatitis virus to non-coding RNAs. Cells. 2021;10(3): 521.
72. Xiu MX, Liu YM, Kuang BH. The oncogenic role of Jagged1/Notch signaling in cancer. Biomed Pharmacother. 2020;129: 110416.
73. Giraud J, Chalopin D, Ramel E, Boyer T, Zouine A, Derieppe MA, et al. THBS1 + myeloid cells expand in SLD hepatocellular carcinoma and contribute to immunosuppression and unfavorable prognosis through TREM1. Cell Rep. 2024;43(2): 113773.
74. Jiang M, Karsenberg R, Bianchi F, van den Bogaart G. CD36 as a double-edged sword in cancer. Immunol Lett. 2024;265:7–15.
75. Blondy T, d'Almeida SM, Briolay T, Tabiasco J, Meiller C, Chéné AL, et al. Involvement of the M-CSF/IL-34/CSF-1R pathway in malignant pleural mesothelioma. J Immunother Cancer. 2020;8(1):e000182.
76. Poudel M, Kim G, Bhattarai PY, Kim JY, Choi HS. Interleukin-34-CSF1R signaling axis promotes epithelial cell transformation and breast tumorigenesis. Int J Mol Sci. 2021;22(5): 2711.
77. Avşar G, Pîr P. An integrated study to decipher immunosuppressive cellular communication in the PDAC environment. NPJ Syst Biol Appl. 2023;9: 56.
78. Ma X, Wang J, Zhuang J, Ma X, Zheng N, Song Y, et al. P4HB modulates epithelial-mesenchymal transition and the β-catenin/Snail pathway influencing chemoresistance in liver cancer cells. Oncol Lett. 2020;20(1):257–65.
79. Weber F, Utpatel K, Evert K, Treeck O, Buechler C. Chemerin and chemokine-like receptor 1 expression are associated with hepatocellular carcinoma progression in European patients. Biomedicines. 2023;11(3): 737.
80. Apostolo D, Ferreira LL, Vincenzi F, Vercellino N, Minisini R, Latini F, et al. From MASH to HCC: the role of Gas6/TAM receptors. Front Immunol. 2024;15: 1332818.
81. Lee HJ, Jeng YM, Chen YL, Chung L, Yuan RH. Gas6/Axl pathway promotes tumor invasion through the transcriptional activation of slug in hepatocellular carcinoma. Carcinogenesis. 2014;35(4):769–75.
82. He L, Zhang J, Jiang L, Jin C, Zhao Y, Yang G, et al. Differential expression of Axl in hepatocellular carcinoma and correlation with tumor lymphatic metastasis. Mol Carcinog. 2010;49(10):882–91.

Publisher's Note